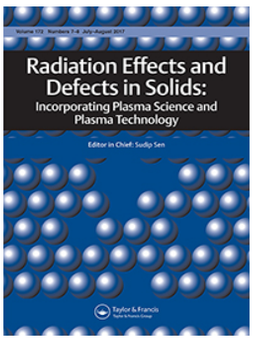

Taylor & Francis
Taylor & Francis Group

Radiation Effects and Defects in Solids
Incorporating Plasma Science and Plasma Technology

ISSN: 1042-0150 (Print) 1029-4953 (Online) Journal homepage: http://www.tandfonline.com/loi/grad20

Axial distribution of plasma fluctuations, plasma parameters, deposition rate and grain size during copper deposition

S. Gopikishan, I. Banerjee, Anand Pathak & S. K. Mahapatra

To cite this article: S. Gopikishan, I. Banerjee, Anand Pathak & S. K. Mahapatra (2017) Axial distribution of plasma fluctuations, plasma parameters, deposition rate and grain size during copper deposition, Radiation Effects and Defects in Solids, 172:7-8, 545-554, DOI: 10.1080/10420150.2017.1359597

To link to this article: https://doi.org/10.1080/10420150.2017.1359597

RADIATION EFFECTS & DEFECTS IN SOLIDS, 2017
VOL. 172, NOS. 7–8, 545–554
https://doi.org/10.1080/10420150.2017.1359597

Taylor & Francis
Taylor & Francis Group

Axial distribution of plasma fluctuations, plasma parameters, deposition rate and grain size during copper deposition

S. Gopikishan[a], I. Banerjee[b], Anand Pathak[c,d] and S. K. Mahapatra[e]

[a]Department of Physics, Birla Institute of Technology, Ranchi, India; [b]School of Nano Sciences, Central University of Gujarat, Gandhinagar, India; [c]School of Physics, University of Hyderabad, Hyderabad, India; [d]Physics Department, Rajiv Gandhi University of Knowledge Technologies (RGUKT)/IIIT Basar, Telangana, India; [e]Centre for Physical Sciences, Central University of Punjab, Bathinda, India

ABSTRACT

Floating potential fluctuations, plasma parameters and deposition rate have been investigated as a function of axial distance during deposition of copper in direct current (DC) magnetron sputtering system. Fluctuations were analyzed using phase space, power spectra and amplitude bifurcation plots. It has been observed that the fluctuations are modified from chaotic to ordered state with increase in the axial distance from cathode. Plasma parameters such as electron density (n_e), electron temperature (T_e) and deposition rate (D_r) were measured and correlated with plasma fluctuations. It was found that more the deposition rate, greater the grain size, higher the electron density, higher the electron temperature and more chaotic the oscillations near the cathode. This observation could be helpful to the thin film technology industry to optimize the required film.

ARTICLE HISTORY
Received 7 January 2017
Accepted 22 July 2017

KEYWORDS
Fluctuation; phase space; power spectrum; electron density; surface morphology; grain size and deposition rate

1. Introduction

DC magnetron sputtering is plasma-based technique used for large scale thin film deposition. It has been used to deposite the size-selected clusters for metals (*1*–*4*), optical coatings (*5*, *6*), hard decorative coatings (*7*), different layers for solar cells (*8*, *9*), biological thin films (*10*, *11*), plasma processing (*12*), memory-based films (*13*), etc. In DC magnetron sputtering system, the magnetron is configured to trap electrons and enhance the ionization of the plasma (*14*–*16*). Furthermore, process parameters such as discharge voltage, pressure, magnetic field and gap of cathode to anode in DC magnetron sputtering system have been used to control the deposition rate, ionization and floating potential fluctuations (FPFs) (*17*, *18*).

A survey of literature reveals that the strength of magnetic field on the plasma affects the deposition rate and energy flux to the substrate in a DC magnetron sputtering system (*19*). Dickson et al. (*20*) has reported that high-density plasma plume exists only at the first few centimeters in front of the target position in conventional magnetron plasma. Radial configuration of plasma gets significantly influenced by the discharge conditions, particularly by the magnetic field intensity (*21*). In chemical vapor deposition, relationship between fluctuations of plasma parameters and the deposited nanomaterial has been

CONTACT S. K. Mahapatra skmahapatra@bitmesra.ac.in

reported (*22*). It is revealed that in dusty plasmas, particles acquire very high dynamic electric charge which brings significant changes in collective behavior of the system (*23*); charge on a grain can fluctuate due to the turbulence or other spatial and temporal variations in the surrounding plasma parameters, in particular the electron temperature (*24*). Different techniques like power spectrum, phase space, bifurcation, self-oscillation, intermittency, period doubling, period subtracting and period adding have been used to analyze nature of FPF(chaotic/order oscillations) (*25*–*28*) and quantified using chaos theories such as Lyapunov exponent, Hurst exponent and entropy estimation (*29*–*34*). FPF of the plasma has been observed in glow discharge, atmospheric and electron cyclotron resonance plasma, whereas, rarely in DC magnetron sputtering plasma.

In the present work, FPFs, plasma parameters and deposition rate were observed axially. FPFs of the plasma have been explained with the help of the power spectrum, phase space and amplitude bifurcation plots. Plasma parameters, deposition rate and grain size were measured axially and correlated with FPF. It was found that more the deposition rate, greater the grain size, higher the electron density, higher the electron temperature and more chaotic the oscillations near the cathode.

2. Experimental details

The schematic diagram of a DC magnetron sputtering system is shown in Figure 1. It consists of (a) DC power supply, (b) source meter, (c) Wilson-seal port, (d) top flange, (e)

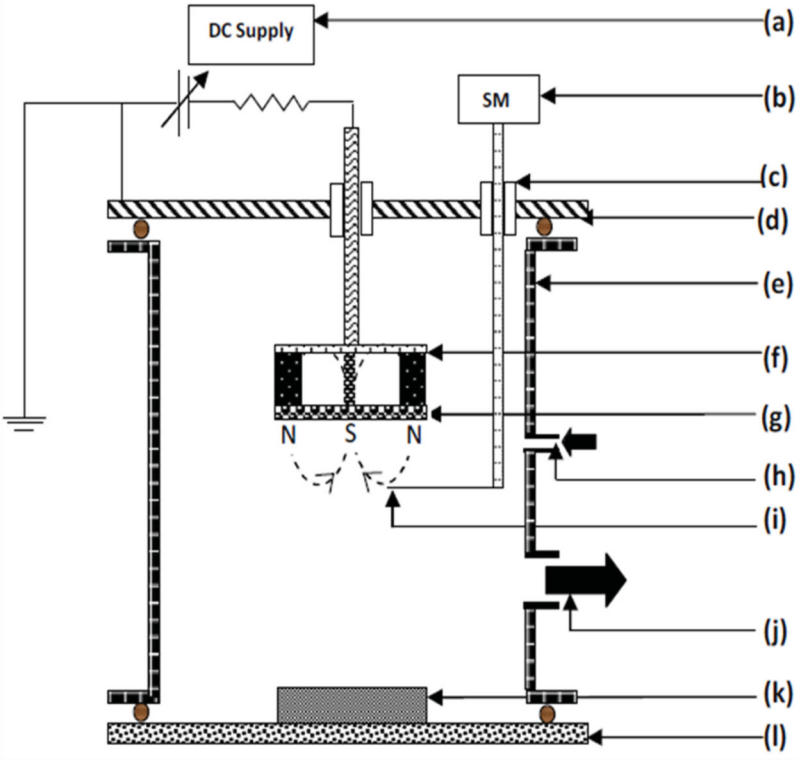

Figure 1. Schematic diagram of DC magnetron sputtering system.

cylindrical shaped stainless steel chamber, (f) magnetron sputter gun, (g) target, (h) MFC gas flow meter, (i) multi Langmuir probe (LP) setup, (j) vacuum pump, (k) substrate holder and (l) bottom flange.

Important part of DC magnetron sputtering system is magnetron sputter gun (f). Diameter of the magnetron is 6 cm. It consists of 13 magnets; 1 magnet is placed at the center (South Pole out of the paper) which is surrounded by 12 other magnets (North Pole out of the paper). All magnets are having identical strength. Cathode, target (g) is clamped to the magnetron sputter gun. A metal cover of the magnetron is isolated by an insulator, this metal cover along with plasma chamber and substrate are act as anode. Negative voltage is applied to the cathode with respect to the metal cover, plasma chamber and substrate as grounded. Top flange is mounted with sputter magnetron and multi LP setup, whereas, bottom flange contains only sample holder.

The chamber was evacuated using a diffusion pump followed by a rotary pump and the base pressure was maintained at $\sim 5 \times 10^{-6}$ mbar. The working pressure was maintained and controlled through mass flow controller (MFC). Process parameters of the DC sputtering plasma are, working pressure (1.1×10^{-2} mbar) at 55 SCCM flow rate of sputtered gas (Ar), discharge voltage (351 volt), target material (Cu). The experiment was performed at four axial distances of 2 cm, 4 cm, 6 cm and 8 cm away from the cathode.

The LP setup consists of a cylindrically shaped tungsten wire of diameter 0.5 mm, mounted on a quartz plate. The probe was connected to the source meter (Keithly 2410, 1100 V). LP setup can be moved up and down without breaking the vacuum into the chamber. LP setup was used to collect the information about the plasma at four different axial positions. At one instant of measurement, the LP setup was positioned at a fixed position and exposed to plasma column. The current vs voltage (I–V) plot was obtained via source meter. Similar measurements were repeated for four axial distances. Electron densities (n_e) and electron temperature (T_e) were estimated from I–V plots. In similar way, FPFs were obtained for four axial distances using digital storage oscilloscope (Agilent Technologies, DSO 1024A). From the plot of floating potential fluctuation, power spectra, phase space and amplitude bifurcation were obtained using time series analyzing techniques.

Four silicon substrates were mounted at the corresponding four axial positions of the LP, where plasma parameters and fluctuations were observed. The area of silicon substrates is 1.2 cm^2 and these are cleaned by diluted HF acid, ultra-sonicated with acetone for 15 min and dried at room temperature prior to deposition. Weights of the bare silicon and deposited silicon were obtained using analytical balance (Mettler Toledo, Germany). Weight difference and deposition time is used to calculate deposition rate (D_r). Surface morphology of deposited samples was obtained using atomic force microscope (AFM), model: solver Pro-47, operation mode: noncontact/tapping mode. The silicon nitride tip was used, with frequency 427 kHz and scan speed was 0.5 Hz. Grain sizes were obtained by the AFM software.

2.1. Results and discussions

FPFs of the plasma have been observed as a function of axial distance from the cathode that is, 2 cm, 4 cm, 6 cm and 8 cm (Figure 2). It is observed that FPF at 2 cm away from the cathode is chaotic in nature. As distance from the cathode increases from 2 cm to 8 cm, the

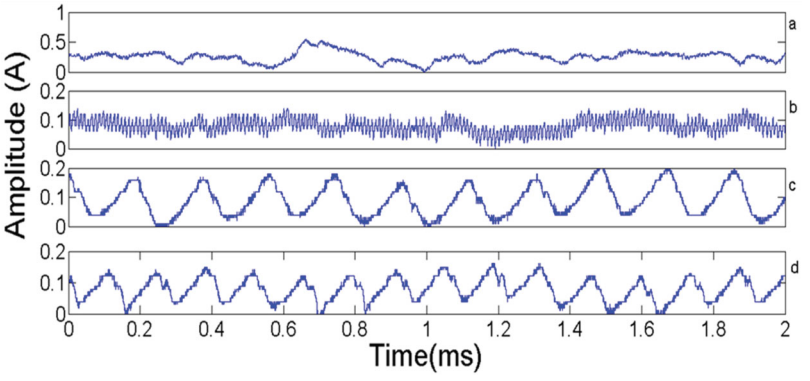

Figure 2. Floating potential fluctuation in plasma at (a) 2 cm, (b) 4 cm, (c) 6 cm and (d) 8 cm axially away from cathode.

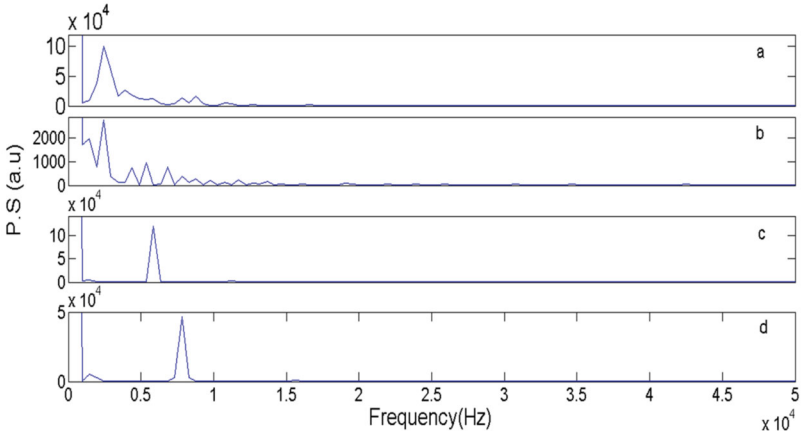

Figure 3. Power spectrum of floating potential in plasma at (a) 2 cm, (b) 4 cm, (c) 6 cm and (d) 8 cm axially away from cathode.

nature of fluctuation is transformed from chaotic to semi periodic. Near the target, higher kinetic energy of electrons may lead to chaotic oscillations.

Figure 3 shows the power spectrum of FPFs shown in Figure 2. Power spectrum plots have been used to get the frequency information present in the system. Power spectra of FPF at 2 cm, 4 cm, 6 cm and 8 cm away from the cathode are shown in Figure 3(a)–(d), respectively. Power spectra at 2 cm and 4 cm axial distances away from the cathode are found to be broad band spectrum whereas predominantly single peaks for 6 cm and 8 cm distances. From this we can conclude that there is a transition of the oscillation from chaotic to ordered state with an increase in the axial distance from the cathode.

Variations of momentum at different position with time have been observed by the phase space plots (PSPs). Phase space plots of the FPFs are shown in Figure 4. It is observed that the shapes of the PSPs are random at 2 cm and 4 cm axial distance from the cathode, whereas, lobe shapes are seen for 6 cm and 8 cm axial distance from the cathode. The literature reports reveal that in ECR plasma, fluctuations change from chaotic-coherent-chaotic

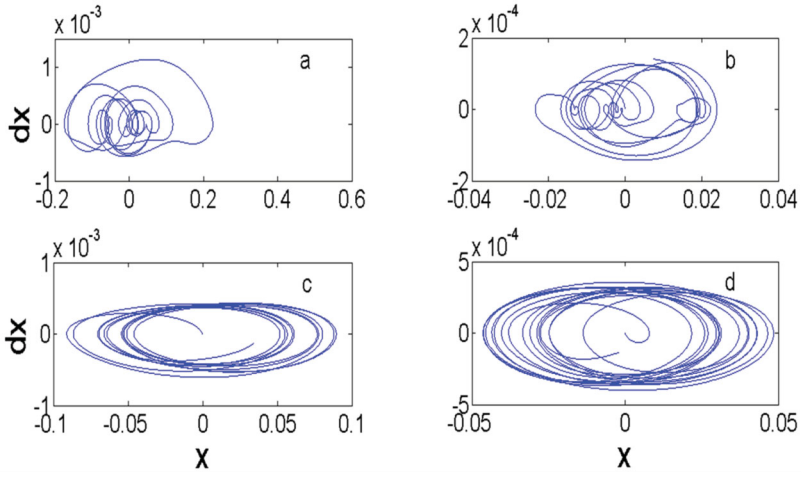

Figure 4. Phase space plots of the FPFs in plasma at (a) 2 cm, (b) 4 cm, (c) 6 cm and (d) 8 cm axially away from cathode.

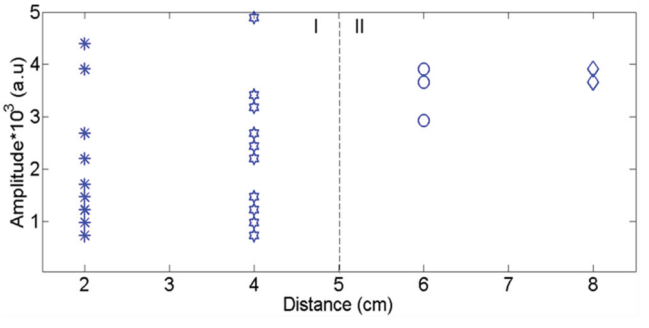

Figure 5. Amplitude bifurcation, bifurcation analysis [S. H. Strogatz et. Al., nonlinear dynamics and chaos book, 44–60 (1994)] comprises the major part of nonlinear dynamics since it can explicate very clearly the performance of the system for a small alter in the value of the control parameter.

as one move radially outwards from the center (*35*). In the present investigations chaotic to order transition of FPFs has been observed as one moves axially outwards from the cathode.

Amplitude bifurcation has been shown in Figure 5. Fluctuations of amplitude are more for 2 cm and 4 cm distance from the cathode, which gradually decreases with increase in the distance. It suggests that the critical distances from the cathode could be divided into two regions as I and II, which is separated by a vertical line in the figure. In region I behavior of the plasma is different than the region II. It is also seen in FPF, power spectrum; in region I fluctuations are chaotic and in region II fluctuations are ordered. Further, physical analysis has been carried out with the help of grain size and plasma parameters in the region I and II.

Thin films were deposited at 2 cm, 4 cm, 6 cm and 8 cm. Figure 6 presents the surface morphology of the thin films. It is observed that the deposited grain size decreases with increase in axial distance from the cathode. Moreover, it is also noticed that each segment of a sample has different grain size and their deviation for each segment is shown in Figure 7.

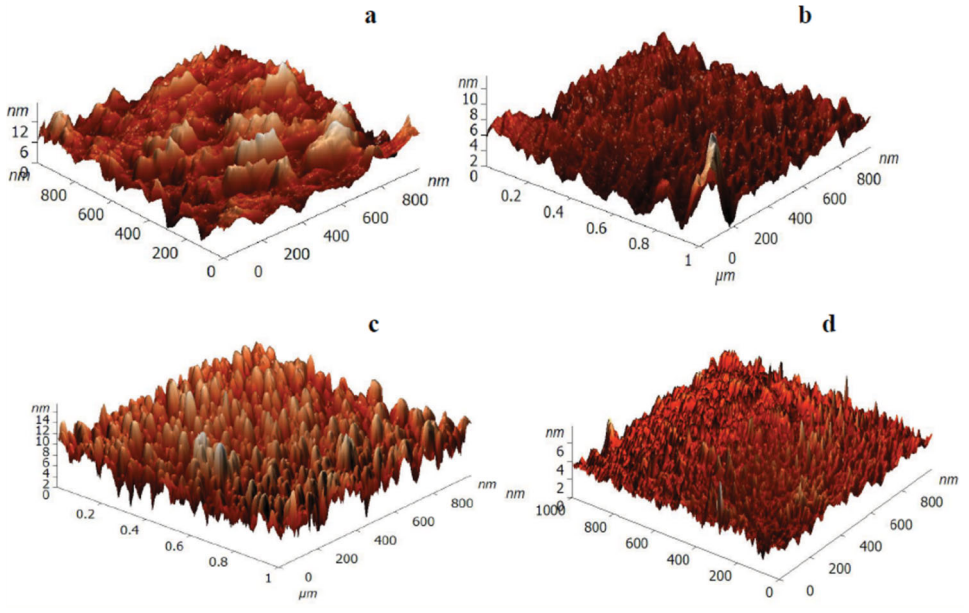

Figure 6. Surface morphology of the copper thin films at (a) 2 cm, (b) 4 cm, (c) 6 cm and (d) 8 cm axially away from cathode.

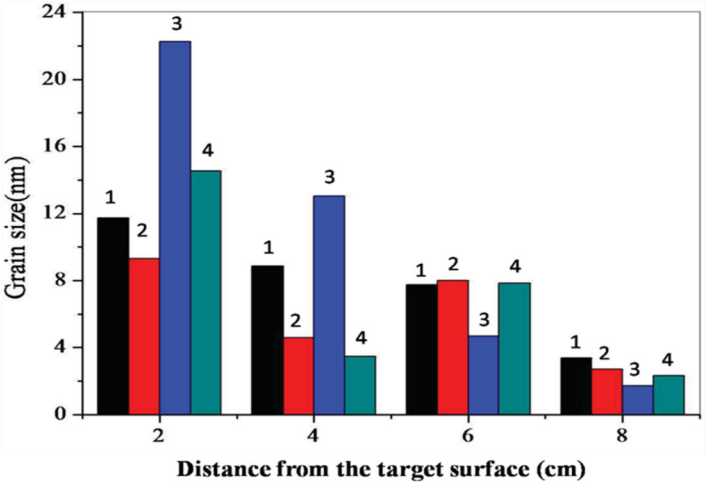

Figure 7. Variation in grain size at (a) 2 cm, (b) 4 cm, (c) 6 cm and (d) 8 cm axially away from cathode.

Grain size was evaluated using the NT-MDT software (NOVA) by threshold calculation of the topographical data and averaged of all the image data. Variation in the grain size of a single sample has been estimated at four different segments and depicted in Figure 7. The actual variation in the grain size for 2 cm, 4 cm, 6 cm and 8 cm of the deposited samples has been shown in this figure. It is observed that average grain size decreases as the axial distance from the cathode increases. Moreover, it is also noticed that each segment of the sample has deviations in grain size as shown in Figure 8.

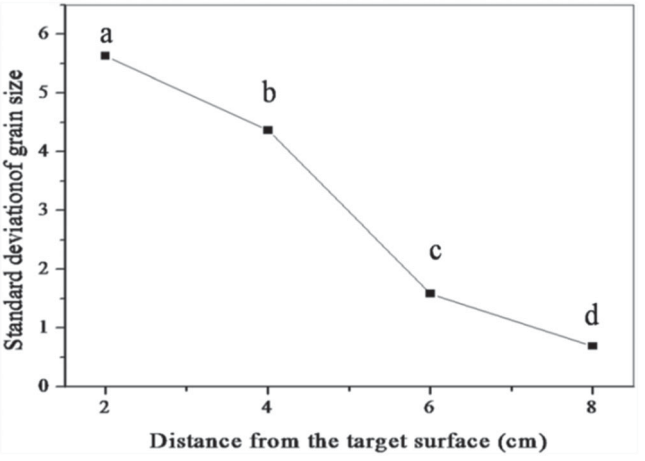

Figure 8. Standard deviation of the grain size at (a) 2 cm, (b) 4 cm, (c) 6 cm and (d) 8 cm axially away from cathode.

Standard deviation σ in the grain size is given by

$$\sigma = \sqrt{\frac{\sum (x - \bar{x})^2}{n - 1}}$$

where x is the grain size of each sample, $\bar{x}$ is the mean value of grain size, n is the number of observations used to estimate standard deviation of the grain. Standard deviation of the grain size is shown in Figure 8. It is found that standard deviation is greater for 2 cm compared to that for 8 cm and higher deposition rate, greater grain size and high electron density near the cathode. This is possibly due to plasma getting trapped in front of the cathode because of the confined magnetic field of the magnetron, and target bombarded by accelerated energetic ions which emits the particles from the target. Magnetic field causes the excited ion energy in front of the cathode (*15*, *36*).

Electron temperature and density were calculated using the following standard relation

$$\frac{\mathrm{d}\ln(I)}{\mathrm{d}V} = \frac{1}{T_{\mathrm{eV}}} \quad \text{and} \quad n_e = \frac{I_{\mathrm{es}}}{eA} \times \sqrt{\frac{K_B T_{\mathrm{eV}}}{2\pi m_{\mathrm{e}}}}$$

where I is probe current, V is probe voltage, and T_{e} is electron temperature, I_{es} is the electron saturation region in the I–V plot, e is the electron charge, A is the area of the probe, K_{B} is the Boltzmann constant, T_{eV} is electron temperature and m_{e} mass of the electron (*37*–*39*). Variations in electron density (n_{e}) and temperature (T_{eV}) are shown in Figure 9(a) and (b), respectively. It is found that both values of n_{e} and T_{eV} are more at 2 cm compared to 8 cm away from the target surface. A similar result was found by applying magnetic strength in a DC magnetron sputtering system (*13*). Reported experimental and theoretical results (*21*, *40*) also indicate similar phenomenon in the system.

The standard relation $D_{\mathrm{r}} = (W_2 - W_1)/(t_2 - t_1)$ where, w_1 is the weight of the bare silicon, w_2 is the weight of the deposited silicon, t_1 is the starting time of deposition, t_2 is the ending time of deposition was used to estimate deposition rate. Deposition rate (D_{r}) was

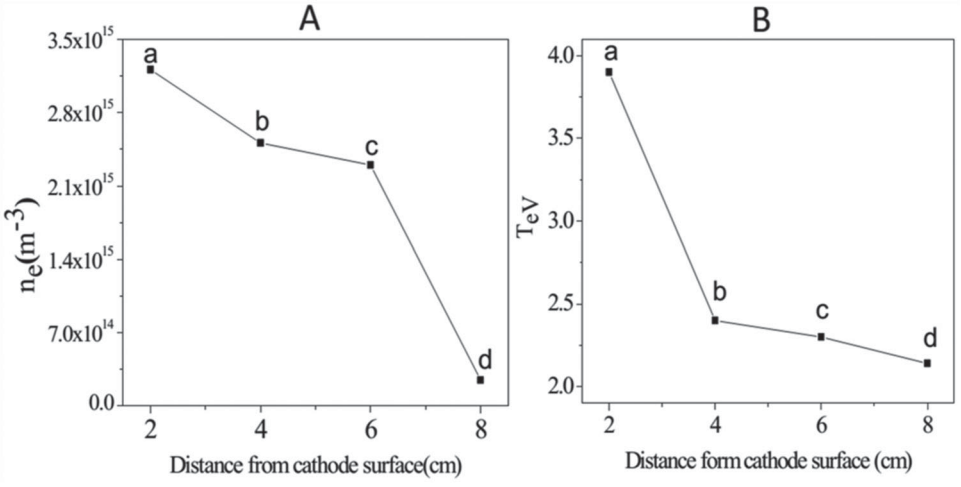

Figure 9. Electron density (n_e) "A"; and electron temperature (T_{eV}) "B"; at (a)2 cm, (f) 4 cm (i) 6 cm and (l) 8 cm away from the cathode.

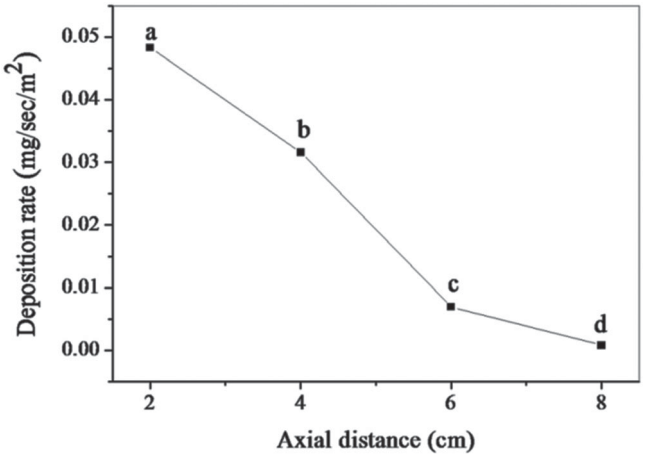

Figure 10. Deposition rate of the thin films at (a) 2 cm, (b) 4 cm, (c) 6 cm and (d) 8 cm axially away from cathode.

estimated at (a) 2 cm, (b) 4 cm (c) 6 cm and (d) 8 cm away from the cathode. Figure 10 shows the D_r at (a) 2 cm, (b) 4 cm (c) 6 cm and (d) 8 cm away from the cathode. It was found that D_r follows similar trend as electron temperature and density variation for axially outward increasing distances from the cathode. Confinement of secondary electrons increases the ionization efficiency, which was the cause for high density and temperature in front of the cathode which results in rapid growth of nanoparticles (*15, 40*). A variation in D_r with magnetic field has been reported (*19, 20*), which are in reasonable agreement with the present observations.

Table 1 shows plasma fluctuations, parameters, deposition rate, correlation between fluctuation and deposition rate, photo of plasma at (a) 2 cm, (b) 4 cm (c) 6 cm and (d) 8 cm

Table 1. Plasma fluctuations, parameters, deposition rate, correlation between fluctuation and deposition rate, photo of plasma at (a) 2 cm, (b) 4 cm (c) 6 cm and (d) 8 cm away from the cathode.

Distance from the target	Instability of the deposited thin films	Axial plasma	Frequency fluctuations of the plasma	Plasma parameters
2cm	Maximum	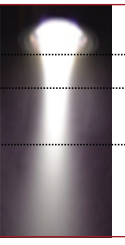	Chaotic	Maximum
4cm	Decreases		Chaotic	Decreases
6cm	Decreases		Order	Decreases
8cm	Minimum (uniform deposition)		Order	Minimum

away from the cathode. The radius of the plasma column gradually changes from the cathode towards the edge region. We see more deposition rate, greater grain size, high electron density, high electron temperature and chaotic oscillations near the cathode.

3. Conclusions

In this paper, we have studied the characteristics of plasma column as a function of axial distance from cathode. Maximum fluctuations are observed near the target. FPFs are found to be chaotic for distances ranging between 2 cm and 4 cm and ordered for 6–8 cm. The grain size of the thin films decreases while moving from the target surface towards the edge region. High density and temperature near the cathode may cause rapid growth in nanoparticles. The plasma parameters are well supported to the FPFs and grain size of the thin films. The deposition rate of the plasma followed the plasma parameters profile. We observed higher deposition rate, greater grain size, high electron density, high electron temperature and chaotic oscillations near the cathode.

Acknowledgements

The authors would like to thank SERB, DST and Government of India for the financial support. S Gopikishan thanks PSSI, IPR Gandhinagar, Gujarat for three-month fellowship. We are thankful to Director, SINP, Kolkata, Prof M. S. Janaki and Prof A. N. Sekar Iyengar for the local hospitality at SINP. APP thanks CSIR for emeritus scientist award.

Disclosure statement

No potential conflict of interest was reported by the authors.

Funding

This work was supported by Science and Engineering Research Board (SERB), Department of Science and Technology (DST), Government of India [grant number EMR/2014/000722].

References

(1) Hartmann, H., Popok, V.N., Barke, I., Von Oeynhausen, V., Meiwes-Broer, K.H. *Rev. Sci. Instrum.* **2012**, *83*, 073304.

(2) Ait Aissa, K., Achour, A., Elmazria, O., Simon, Q., Elhosni, M., Boulet, P., Robert, S., Djouadi, M.A. *J. Phys. D: Appl. Phys*. **2015**, *48*, 145307.
(3) Luo, Z., Woodward, W.H., Smith, J.C., Castle Man Jr, A.W. *Int. J. Mass. Spectrum*. **2012**, *309*, 176–181.
(4) Greczynski, G., Jensen, J., Hultman, L. *IEEE Transactions on Plasma Science*. **2010**, *38*, 3046–3056.
(5) Steglich, M., Patzig, C., Berthold, L., Schrempel, F., Fuchsel, K., Hoche, T., Kley, E.B., Tunnermann, A. *AIP Adv*. **2013**, *30*, 72108-8.
(6) Wu, S.Z. *J. Appl. Phys*. **2005**, *98*, 083301-5.
(7) Jacobsohn, L.G., Prioli, R., Freire Jr, F.L., Mariotto, G., Lacerda, M.M., Chung, Y.W. *Diamond Relat Mater*. **2000**, *9*, 680–684.
(8) Cebulla, R., Wendt, R., Ellmer, K. *J. Appl. Phys*. **1998**, *83*, 1087–1095.
(9) Nedfors, N., Tengstrand, O. *Thin Solid Films*. **2013**, *545*, 272–278.
(10) Chen, W., Liu, Y., Courtney, H.S., Bettenga, M., Agrawal, C.M., Bumgardner, J.D., Ong, J.L. *Biomaterials*. **2006**, *27*, 5512–5517.
(11) Panda, A.B., Gopikishan, S., Mahapatra, S., Barhai, P.K., Das, A.K., Banerjee, I. *Ceram. Int*. **2014**, *40*, 4681–4690.
(12) Li, H., Zheng, Y., Pei, Y.T., De Hosson, J.Th.M. *J. Mater. Sci.: Mater. Med*. **2014**, *25*, 1249–1255.
(13) Ekpe Samuel, D., Jimenez Francisco, J., Field David, J., Davis Martin, J., Dew Steven, K. *J. Vac. Sci. Technol. A*. **2009**, *27*, 1275–1280.
(14) Goeckner, M.J., Goree, J.A., Sherdian, T.E. *IEEE Trans. Plasma Sci*. **1991**, *19*, 301–308.
(15) Borah, S.M., Bailung, H., Ratan Pal, A., Chutia, J. *J. Phys. D: Appl. Phys*. **2008**, *41* 195205.
(16) Hun Seo, S., Hwan In, J., Young Chang, H., Dickson, M., Hopwood, J. *J. Appl. Phys*. **2004**, *96*, 57–64.
(17) Pankaj Kumar, S., Debajyoti, S., Sabuj, G., Janaki, M.S., Sekar Iyengar, A.N. *Chaos*. **2015**, *25*, 043101-6.
(18) Thornton, J. *J. Vac. Sci. Technol* **1974**, *11*, 666–670.
(19) Hellgren, N., Macak, K., Broitman, E., Johansson, M. P., Hultman, L., Eric Sundgren, J. *J. Appl. Phys*. **2000**, *88*, 524–532.
(20) Dickson, M., Hopwood, J. *J. Vac. Sci. Technol. A*. **1997**, *15*, 2307–2312.
(21) Peres, I., Fortin, M., Margot, J. *Phys. Plasmas*. **1996**, *3*, 1754–1769.
(22) Masaharu, S., Kazunori, K., Kunihiro, K., Shinya, I., Giichiro, U., Hyunwoong, S., Naho, I. *Jpn. J. Appl. Phys*. **2014**, *53*, 010201-4.
(23) Li, K.M., Kang, L.F., Wang, C.Y., Li, X., Huang, W.Z. *Indian J. Phys*. **2014**, *88*, 1207–1210.
(24) Cui, C., Goree, J. *IEEE Trans. Plasma Sci*. **1994**, *22*, 151–158.
(25) Qin, J., Wang, L., Yuan, D.P., Gao, P., Zhang, B.Z. *Phys. Rev. Lett*. **1989**, *63*, 163–166.
(26) Cheung, P.Y., Donovan, S., Wong, A.Y. *Phys. Rev. Lett*. **1988**, *61*, 1360–1363.
(27) Cheung, P.Y., Wong, A.Y. *Phys. Rev. Lett*. **1987**, *59*, 551–554.
(28) Nurujjaman, M.D., Sekar Iyengar, A.N. *Pramana*. **2006**, *67*, 299–304.
(29) Hassouba, M. A., Al Naggar, H. I., Al Naggar, N. M., Wilke, C. *Phys. Plasmas*. **2006**, *13*, 073504.
(30) Lahiri, S., Roy Chowdhury, D., Sekar Iyengar, A.N. *Phys. Plasmas*. **2012**, *19*, 082313.
(31) Debajyoti, S., Pankaj Kumar, S., Janaki, M.S., SekarIyengar, A.N., Sabuj, G., Vramori, M., Michael Wharton, A. *Phys. Plasmas*. **2014**, *21*, 032301-7.
(32) Nurujjaman, Md., Sekar Iyenga, A.N. *Phys. Lett. A*. **2007**, *360*, 717–721.
(33) Bornali, S., Sourabh, C., Wharton, A.M., Sekar Iyengar, A.N. *Phys. Scr*. **2014**, *88*, 065005-10.
(34) Chowdhury, D.R., Iyengar, A.N.S., Lahiri, S. *Nonlin Proc. Geophys*. **2012**, *19*, 53–56.
(35) Subir, B., Iyengar, A.N.S., Rabindranath, P. *Phys. Plasmas*. **2012**, *19*, 032310-6.
(36) Gopikishan, S., Pankaj Kumar, S., Sekar Iyengar, A.N., Banerjee, I., Mahapatra, S.K. *Phys. Plasmas*. **2015**, *22*, 082121-5.
(37) Merlino, R.L. *Am. J. Phys*. **2007**, *75*, 1078–1085.
(38) Singh, S.B., Chand, N., Patil, D.S. *Vacuum*. **2008**, *83*, 372–377.
(39) Field, D.J., Dew, S.K., Burrell, R.E. *J. Vac. Sci. Technol A*. **2002**, *20*, 2032.
(40) Misina, M., Setsuhara, Y., Miyake, S. *J. Vac. Sci. Technol. A*. **1997**, *15*, 1922–1928.